RSC Advances

Microwave-assisted synthesis and deposition of a thin ZnO layer on microwave-exfoliated graphene: Optical and electrochemical evaluations

Journal:	*RSC Advances*
Manuscript ID:	RA-ART-05-2015-009936.R1
Article Type:	Paper
Date Submitted by the Author:	17-Jul-2015
Complete List of Authors:	Kumar, Rajesh; State University of Campinas (UNICAMP), Campinas, Sao Paulo, Brazil, Centre for Semiconductor Components Singh, R; Banaras Hindu University, Physics;

Graphical Abstract

During the microwave irradiation, situ process GO transform into MpEG with porous nanostructure and at the same time, zinc nitrate decomposed into Zn^{2+} ions. The MpEG have some functional group on the surfaces which behaves similar to negative charges. The Zn^{2+} ions get attracted towards negative functional group and are attached on the MpEG. The Zn^{2+} reacts with the functional groups on the MpEG, leading to the local creation of Zn–O–C and Zn-O bonding and bind on MpEG sheets. Zn^{2+} transferred into ZnO nanoparticles by the help of oxygen content in the functional group on the MpEG sheets by absorbing thermal energy from microwave irradiation. Whole MpEG sheets are attracted towards ZnO nanoparticles in which functional group plays crucial role to bring them nearer to each other and the final structure formation of ZnO_L@MpEG hybrids.

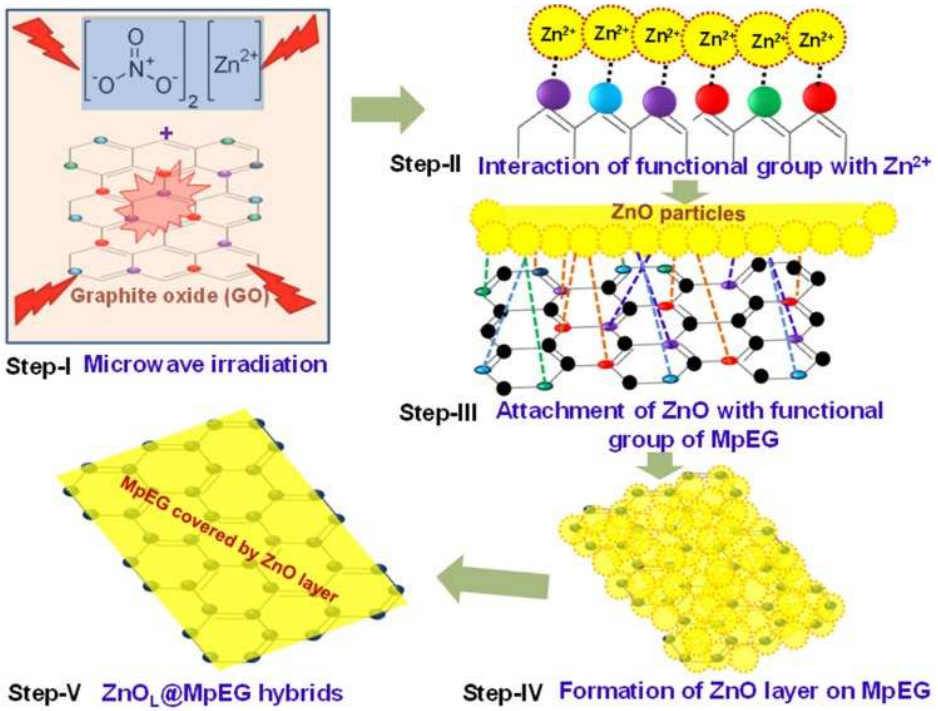

Figure 1: Mechanism of the formation of ZnO_L@MpEG hybrids in different stage with functional group present on the MpEG sheets.

RSC Advances

ARTICLE

Microwave-assisted synthesis and deposition of a thin ZnO layer on microwave-exfoliated graphene: Optical and electrochemical evaluations

Received 00th January 20xx,
Accepted 00th January 20xx

DOI: 10.1039/x0xx00000x

www.rsc.org/

Rajesh Kumar*[a], Rajesh Kumar Singh*[b], Alfredo R. Vaz [a], Stanislav A. Moshkalev [a]

A rapid and facile microwave-assisted method has been developed for the deposition of zinc oxide layer (ZnO_L) in-situ on partially microwave exfoliated graphene (MpEG). For the formation of ZnO layer on microwave partially exfoliated graphene (ZnO_L@MpEG) hybrids, only requires zinc nitrate and MpEG sheets react under a low level of microwave irradiation (700 W) for 5 min. The deposited thin ZnO_L on MpEG sheets are uniformly well-dispersed and cover the whole MpEG sheets. The as-prepared ZnO_L@MpEG) hybrids demonstrate the enhanced electrochemical properties as supercapacitor and also show quenching phenomena for photoluminescence. The fluorescent quenching was observed for the ZnO_L@MpEG hybrids compared to ZnO, indicates the photo induced electron transfer from ZnO to MpEG layers, which shows the recombination of hole and electron charge carriers. The electrochemical measurement exhibited that the ZnO_L@MpEG hybrids have large integral area of cyclic voltammetry loop, indicating that such hybrids is promising for application in supercapacitors. The material displayed a high specific capacitance of 347 F/g at a current density of 5.0 A/g. The mechanism for the formation of the ZnO_L@MpEG hybrids via the microwave method has also been proposed.

Introduction

As a new class of energy storage device supercapacitors, also known as electrochemical capacitors, has received considerable attention. Supercapacitors can be used in hybrid electric vehicles, memory backup, and other emergency power supply devices due to their higher power density, superior cycle lifetime, and low maintenance cost[1-4]. Graphene and ZnO are two of the most widely studied nanomaterials; both of them are good candidates for the electrode materials of supercapacitors[5-7]. As we know that hybrid nanostructure of low-dimensional semiconductor as ZnO with two-dimensional (2-D) graphene layers are emerging as a new materials for fabricating transferable or flexible optoelectronic and electronic devices. Among various semiconductors, zinc oxide nanoparticles process excellent characteristics in providing photocatalytic [8, 9], photonic [10], spintronics [11] photoluminescence quenching [12] and electronic [13] properties primarily due to its wide band gap (3.37 eV) and high exciton binding energy of 60 meV [14, 15]. The ZnO nanostructures work as efficient channels for carrier transport and electrical pumping to radiative recombination, thereby improving the device performances incredibly in optoelectronics and electronics. The graphene, which have astounding thermal and electrical conductivity, high mechanical strength and elasticity, and optical transparency, act as novel substrates offering new functionalities, for example, transferability or adaptability. Graphene, is the most recent new nano carbon material, is viewed as a stand out amongst the most promising addictive for hybrid materials, on account of its substantial theoretical specific surface area, excellent electron mobility, and high transparency [16, 17]. Meanwhile, incorporating ZnO with reduced graphene oxide (rGO) not only can reduce the restocking of ultrathin graphene sheets, but also can prevent the combination of electron-hole pair and aggregation in photoluminescence. Recently, numerous ZnO-graphene hybrid nanostructures have been endeavored to enhance its performances in the versatile applications. Also, graphene-based ZnO hybrids have been fabricated by several methods including electrochemical deposition of ZnO on rGO [18], rGO decorated ZnO by hydrolysis-calcination [19], graphene-ZnO nanorod heterostructure by hydrothermal approach [19], graphene-multipod nanocomposite using hydrothermal processes [20] and graphene-ZnO nanocomposite employing microwave irradiation [5-7, 21] for various applications. Such type of graphene-ZnO nanostructures shows synergistic effects in electrochemical [6, 7, 22], optical properties [23] and photo-catalytic [9, 21, 24, 25] applications.

However, in this work we have carried out one-step synthesis process for ZnO_L@MpEG hybrids and its application as electrode materials as well as photoluminescence properties. In this synthesis process microwave-assisted deposition of ZnO layer has been done on microwave partially exfoliated graphene (MpEG) sheets. This microwave irradiation method has advantages, such as simple, low cost and easy to scale up. This method for synthesis of ZnO_L@MpEG can produce heat to the reactant to a high temperature in a very short time by transferring energy Thus it can facilitate the reaction

[a] Centre for Semiconductor Components, State University of Campinas, Campinas, Sao Paulo 13083-870, Brazil. E-mail: rajeshbhu1@gmail.com
[b] Department of Physics, Indian Institute of Technology (Banaras Hindu University), Varanasi-221005, India. E-mail: rksbhu@gmail.com

† Footnotes relating to the title and/or authors should appear here. Electronic Supplementary Information (ESI) available: [details of any supplementary information available should be included here]. See DOI: 10.1039/x0xx00000x

in situ in a short time with small energy cost [22, 26-28]. The ZnO_L@MpEG hybrids show the enhanced electrochemical behaviour and optical quenching properties.

Experimental

Preparation of graphite oxide (GO) and microwave exfoliated partially exfoliated graphene (MpEG)

GO was prepared using graphite powder according to slightly modified Staudenmaiers method [19]. Graphite powder was put into the solution of conc. H_2SO_4 (36 ml) and HNO_3 (18ml) at room temperature under magnetic stirring condition. After that, the solution was put into an ice-water bath to ensure constant temperature and potassium chlorate was slowly poured to avoid the explosion due to exothermic reactions. Now this solution was put at room temperature for five days under magnetic stirring for better oxidation of graphite powder. As obtained GO solution was washed with DI water and 10% HCl solution was added to remove sulphate and other ion impurities. It was washed with DI water until its show pH 7. After than GO powder was dried at 70° C under vacuum. 10 mg of dried GO powder was converted into MpEG sheets by the help of microwave irradiation (700 W, 1 minute) for the comparative study of electrochemical and optical evaluations.

Synthesis of ZnO layer on MpEG (ZnO_L@MpEG) hybrids

The ZnO_L@MpEG hybrids nanostructure was prepared by the microwave irradiation. First GO (20 mg) and zinc nitrate [$(Zn(NO_3)_2$] (1.5 mg) were mixed in DI water (70 ml) with vigorous stirring for 50 min to get uniform dispersion and suspension. Magnetic stirring was done at room temperature in 250 ml flask. After that, 10 ml $NH_3.H_2O$ (0.2 M) solution was added slowly into the flask drop wise over 20 minutes with intense stirring. Afterward, the mixture solution was sonicated for 5 minutes and then put into oven at 50 ^{0}C for over night. After complete evaporation of solution, the powder was microwave irradiated for 5 min. After complete evaporation of solution, the powder was microwave irradiated at 700 W for 5 min. The microwave irradiation was carried out in a domestic microwave (MS2021CW) oven manufactured by LG.

Materials characterization

The morphologies and the microstructure of the synthesized products were analyzed using Scanning electron microscope (Philips XL 20) and high-resolution transmission electron microscope (HRTEM, FEI Tecnai G20, FEI Company, USA). The elemental compositions, the crystalline structures and bonding information of the synthesized products were analyzed using an X-ray diffraction (XRD, D/MAX- 2500/PC; Rigaku Co., Tokyo, Japan), energy dispersive spectrometer (EDS, FEI Tecnai G20, FEI Company, USA), and X-ray photoelectron spectroscopy (XPS, Axis Ultra, Kratos Analytical Ltd., England), respectively. Whereas it's optical absorption properties were investigated using a UV/vis diffuse reflectance spectrophotometer (U-41000; HITACHI, Tokyo, Japan).

Electrochemical measurements

The cyclic voltammetry (CV) and charge discharge measurements were done in a three-electrode system, for the calculation of specific capacitance. The as-prepared hybrid materials was used as working electrode, platinum (Pt) wire as counter electrode and Ag/AgCl as reference electrode. The measurements were carried out in a 1.0 M Na_2SO_4 solution as electrolyte at room temperature. Electrochemical measurements, such as CV and charge-discharge were carried out by a VersaSTAT 3 (Princeton Applied research). The glassy carbon electrodes (GCEs) (5 mm diameter) were polished with 1.0 and 0.05 mm alumina slurry. Afterwards it was sonicated in ethanol for cleaning and removal of contaminations. 1.0 mg of the electrode materials was dispersed in 1.0 mL of dimethylformamide (DMF) with the aid of ultrasonicator to give a 1.0 mg/mL black suspension. Then, 10 µL of the black suspension was dropped on a cleaned GCE electrode with the help of a micro-syringe and the solvent was left to evaporate in air for 1 hr at room temperature. Thus, a uniform film of electrode materials coating gets formed on the surface of GCE. Finally, 5 µL of nafion (5 wt. %) was cast and used as a net to stably hold the materials on the electrode surface stably. The solvent was allowed to evaporate before use and the final electrode was taken for the electrochemical measurements.

Result and discussion

The XRD pattern of ZnO_L@MpEG hybrids nanostructures is shown in Figure 1. The diffraction peaks of ZnO_L@MpEG hybrids appears at 2θ values of 31.9 °, 34.5 °, 36.4 °, 47.6 °, 56.6 °, 62.9 °, 66.5 °, 68.1 ° and 69.2 °. All these characteristic diffraction peaks can be indexed to the ZnO hexagonal Wurtzite structure of (100), (002),

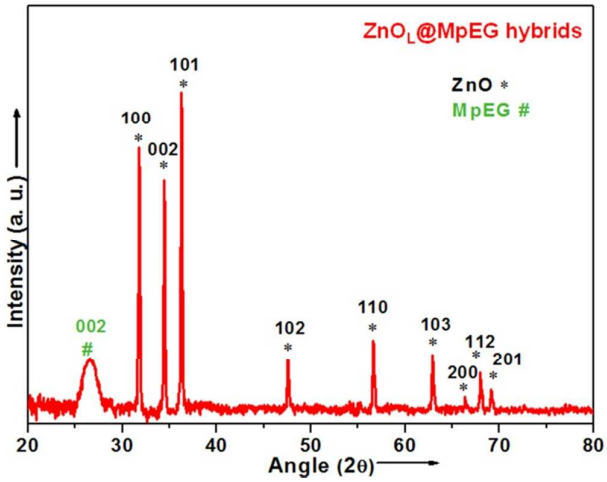

Figure 1: X-ray diffraction pattern of as synthesized ZnO_L@MpEG hybrids.

(101), (102), (110), (103), (200), (112) and (201) planes, which match well with the standard ZnO peaks (JCPDS 36-1451) [29]. The (002) peak of MpEG also appears nearly 26.5 °, in the as synthesized ZnO_L@MpEG hybrids nanostructure. The MpEG shows single and broad diffraction peaks at 2θ=26.5°, which is attributed to the (002) reflections of graphitic carbon, respectively. The broader peak at 26.5° indicates an interlayer space of 0.34 nm, which is similar to the natural graphite but is distinct to the commonly used defective graphene oxide [30]. No characteristic peaks of other impurities, such as $Zn(OH)_2$ [29], were detected in the XRD patterns. The XRD pattern of the ZnO_L@MpEG hybrids indicates that the ZnO nanostructures formed on graphene have high crystallinity.

The SEM morphology of the as-synthesized MpEG and ZnO_L@MpEG hybrids nanostructures are shown in Figure 2. Figure 2a, shows wrinkles and fluffy-like structure in the as synthesized

MpEG and folds at edges with lateral dimensions of several microns with voids as covered by the graphene sheets. Figure 2b,c and c show the SEM micrograph of ZnO_L@MpEG hybrids at different magnifications. This ZnO_L@MpEG hybrid nanostructure clearly shows that ZnO nanoparticles are uniformly deposited on the MpEG surfaces. It can be clearly observed that MpEG sheets are attached densely by ZnO nanoparticles, which display a good combination between MpEG and ZnO. No significant structural changes appear after the deposition of ZnO nanoparticles. From the image of ZnO_L@MpEG hybrids in Figure 2c, subtle-layered structure can be observed in SEM micrographs. However, the layered structure is rather non-uniform. The surface of MpEG is completely covered by a mass of ZnO nanoparticles. We can infer that a layer of ZnO nanoparticles distributes on the external and internal surfaces of MpEG sheets.

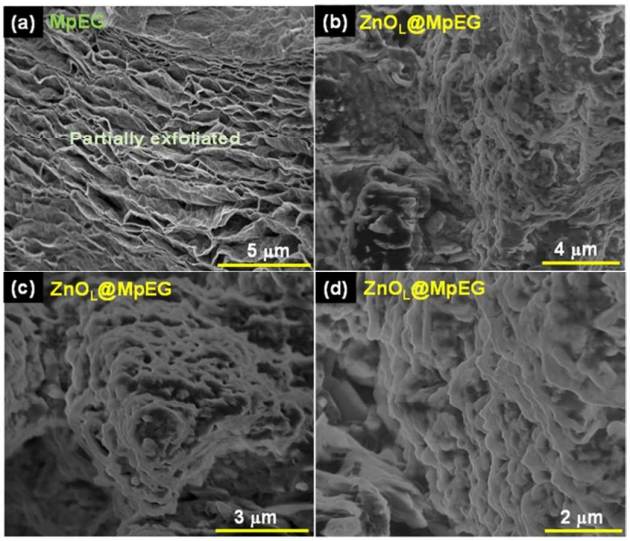

Figure 2: SEM micrograph of as synthesized (a) MpEG and (b,c d) ZnO_L@MpEG hybrids.

The Microstructural morphology of ZnO_L@MpEG hybrids is further investigated by HRTEM. Figure 3 shows the HRTEM morphologies of the as prepared MpEG and ZnO_L@MpEG hybrids samples. HRTEM morphology of the MpEG prepared by microwave reduction has been shown in Figure 3a. Figure 3a, shows the transparent nature and wrinkles on the surfaces. The π-π network of graphene-based systems makes them good electron acceptors. The surfaces of MpEG are rough on the nanoscopic scale with some wrinkles, which may be attributed to the residual functional groups present on the surfaces and the resultant defects produced during the preparation of MpEG. Figure 3b,c, and d shows the ZnO_L@MpEG hybrids consisting of a layer of fine ZnO nanoparticles on the MpEG sheets. As can be seen from Figure 3b,c, the ZnO nanoparticles are very small in size and are evenly distributed. The existence of ZnO in ZnO_L@MpEG hybrids have also been proved by the peaks of Zn and O in energy dispersive spectroscopy (EDS) data. The EDS (Inset of Figure 3c) results show that carbon (C), oxygen (O), zinc (Zn), and copper [31] elements are present in the Zn_L@MpEG hybrids. The atomic percentage of C, O, and Zn were 74, 20 and 5.7, respectively. Figure 3d, shows the HRTEM microscopic morphology of the ZnO nanoparticles under high magnification. The ZnO nanoparticles in ZnO layers are not agglomerated on the surface of MpEG and shows polycrystalline nature which can be seen in Figure 3d. The particles size of ZnO in the ZnO_L@MpEG hybrids is about 5-20 nm. The (002) crystal plane of ZnO with a d spacing of approximately 0.26 nm is clearly observed in the inset of Figure 3d. It is confirmed by HRTEM as shown in Figure 3d, ZnO nanoparticles are fairly dispersed on the surface of MpEG. This shows an intimate contact between the ZnO layer and MpEG sheets.

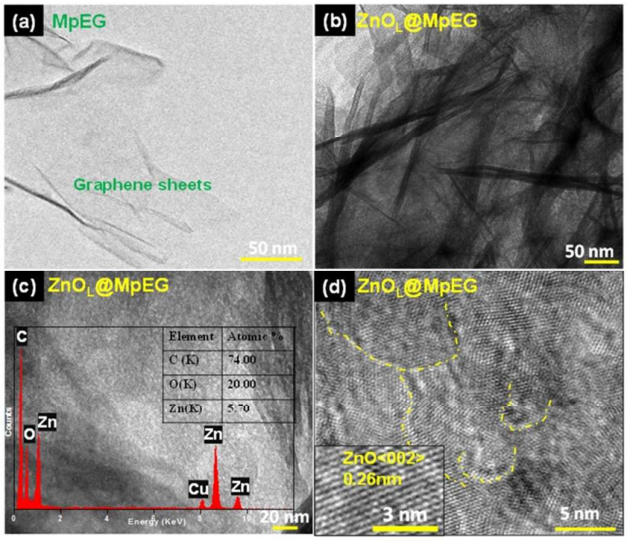

Figure 3: TEM micrograph of as synthesized (a) MpEG and (b,c,d)ZnO_L@MpEG hybrids. Inset of Figure 3c shows the EDS of ZnO_L@MpEG hybrids.

Raman spectroscopy is an effective technique to investigate the structure, crystallization, and defects in the ZnO_L@MpEG hybrids materials. Figure 4 displays the typical Raman spectrum of the hybrid nanostructure materials between the ranges of 200-3000 cm^{-1}. In Figure 3a, MpEG exhibited D band at 1374 cm^{-1} and G band at 1590 cm^{-1}. After formation of ZnO_L@MpEG hybrids materials, the D band and G band gets shifted to 1364 and 1597 cm^{-1}. It may be noted that the Raman D-band peak of MpEG at 1374 cm^{-1} has shifted to 1364 cm^{-1} in ZnO_L@MpEG hybrids, i.e. shifted towards the lower wave number. The Raman G peak of MpEG at 1590 cm^{-1} has shifted to 1597cm^{-1} in ZnO_L@MpEG hybrids i.e. is shifted towards the higher wave number. These observations show that the D band has been slightly red-shifted by 10 cm^{-1} in the ZnO_L@MpEG hybrids, while the G band has shown a blue shift of 7 cm^{-1}. The 2D band is also shifted from 2684 cm^{-1} to 2677 cm^{-1} in ZnO_L@MpEG hybrids. The different positions of D, G and 2D bands of pristine MpEG and ZnO_L@MpEG hybrids suggest that a strong interaction occurs between pristine MpEG and ZnO in the ZnO_L@MpEG hybrids either by chemical bonding with functional groups of graphene or by surface deposition. The I_D/I_G (intensity ration of D and G band) was 0.94 for MpEG and 1.09 for ZnO_L@MpEG hybrids material, in which the increase of I_D/I_G suggest an increase in disorder due to the incorporation of ZnO nanoparticles into the graphene layers of MpEG. The peaks towards lower wave number side of ZnO_L@MpEG hybrids, located at 681 cm^{-1} and 462 cm^{-1} are ascribed to the A_1 (LO) modes and E_2 (high) phonons of ZnO nanorods, respectively which are characteristics of

ZnO nanoparticles. [23, 32]. The surface composition and the chemical states can be determined by the XPS spectrum according to the corresponding binding energies of the different elements in the materials.

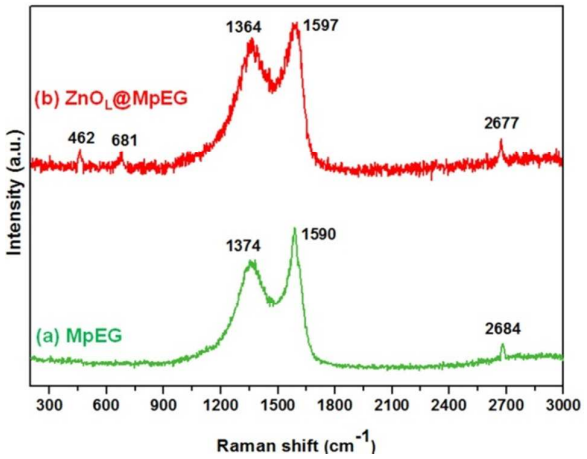

Figure 4: Raman spectra of (a) MpEG and (b) ZnO$_L$@MpEG hybrids.

Figure 5a show the XPS spectra of ZnO$_L$@MpEG hybrids and it indicates the presence of three dominative elements as C, Zn and O is 73.52, 21.29 and 5.12 (at. %), respectively. The additional weak peak of N in ZnO$_L$@MpEG hybrids appeared due to the incorporation of ammonia. Figure 5b, show the deconvoluted XPS C1s spectra which exhibits three components: C-C (284.6 eV), C-O (285.8 eV) and C=O (288.3 eV) [33]. The XPS spectra of the Zn-2p core level regions have been shown in Figure 5c. The ZnOL@MpEG hybrid displays a doublet at about 1021.6 and 1045 eV, corresponding to the Zn $2p_{3/2}$ and $2p_{1/2}$ core levels [31]. The binding energy difference between the two lines is 23.4 eV, which is well lying within the standard reference value of ZnO [34]. The first peak is attributed to Zn^{2+} ions in the oxygen-deficient ZnO matrix [35].

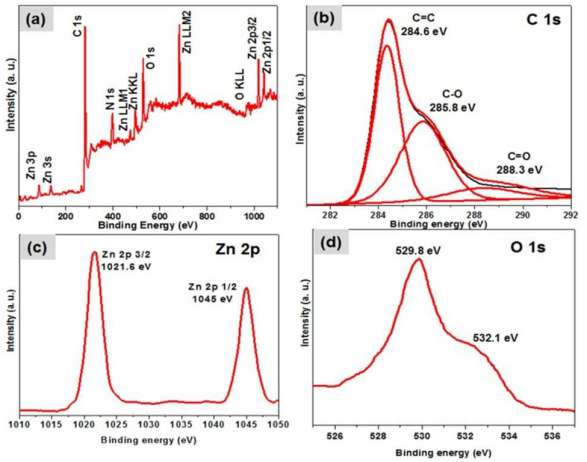

Figure 5: XPS spectra as (a) complete survey, (b) C 1s, (c) Zn 2p, and (d) O 1s core level of ZnO$_L$@MpEG hybrids.

Moreover, the all of Zn $2p_{3/2}$ XPS peaks are sharp. Thus, it can be confirmed, that Zn element exists mainly in the form of Zn^{2+} on the samples surfaces [30, 36]. This evidence confirms the presence of formation of ZnO in as synthesized hybrids. Figure 5d display the XPS spectra of O 1s region of the ZnOL@MpEG hybrids. The O 1s core-level spectrum shows two different forms of oxygen. The lower binding energy of 529.8 eV, and is assigned to oxygen ions in the Zn-O bonding of the wurtzite structure of ZnO [37]. The other peak located at 532.1 eV is related to OH group absorbed onto the surface of the ZnO nanoparticles [38].

The improvement in charge carrier separation and the prolonged lifetime of photo generated electron–hole pairs can be confirmed by the PL spectra. PL spectra provide the separation and recombination information of the photo induced electrons and holes in the material. It is demonstrated that the unique ZnO$_L$@MpEG hybrids features of MpEG and ZnO make it capable to improve the lifetime of photo excited electron–hole pairs generated from ZnO layer and in result boost the efficient transfer of charge carriers. This statement is supported by the analysis of photoluminescence (PL) spectra. Figure 6 exhibits the PL spectra of the MpEG and ZnO$_L$@MpEG hybrids material. It is found that ZnO is a good electron donor and the carbon materials such as MpEG are relatively good electron acceptors. Thus, the synergistic effect between these two, MpEG and ZnO layer would effectively reduce recombination of photo generated electron–hole pairs from ZnO and lead to an increased charge carrier separation [39]. Figure 6 shows the PL spectra of ZnO, under excitation wavelength of 350 nm (Xe lamp), there is one weak peak of UV emission around 380 nm (near band edge (NBE) emission of ZnO). The peak emission at 380 nm can be described as the recombination of the charge carriers near the band edges of ZnO. The other strong and broad green emission with a peak at 580 nm is also detected, which can be attributed to the surface defect and oxygen vacancies in ZnO lattice [40, 41]. This 580 nm emission peak can be assigned to the electron excited-recombined on the surface of ZnO nanoparticles. For the ZnO$_L$@MpEG hybrids, the obviously decreased emission intensity represents an effective interfacial charge transfer process, suggesting that an additional pathway dominates for the disappearance of the charge carriers, because of the interactions between the excited ZnO and MpEG [42, 43]. This indicates that the nanostructure has a lower recombination rate of electrons and holes under UV light irradiation, which is mainly due to the fact that the electrons are excited from the valence band of ZnO to the conduction band and then transfer to MpEG sheets, preventing a direct recombination of electrons and holes. Apparently, the fluorescence emission intensity of ZnO$_L$@MpEG hybrids was significantly quenched, suggesting an additional passage for the charge carriers due to the strong interactions between ZnO and the MpEG sheets[43,44]. This result also suggested the efficient interaction between ZnO and MpEG, which indicated more separation of photo induced electrons and holes by the addition of MpEG. Inset of Figure 6 shows the possible mechanism for the charge transfer and separation in the ZnO$_L$@MpEG hybrids. When UV light is incident on ZnO, the excited electrons jump from the valence band (E_{VB} = - 7.25 eV) of ZnO to its conduction band (E_{CB} = - 4.05 eV), but these electrons can combine with holes quickly (recombination not shown here). In ZnO$_L$@MpEG hybrids, due to the interaction between ZnO and MpEG sheet, the electrons from ZnO easily gets transferred to the surface of graphene sheets (work function of graphene φ = – 4.42 eV) and delay the combination of electron and hole [40, 45].

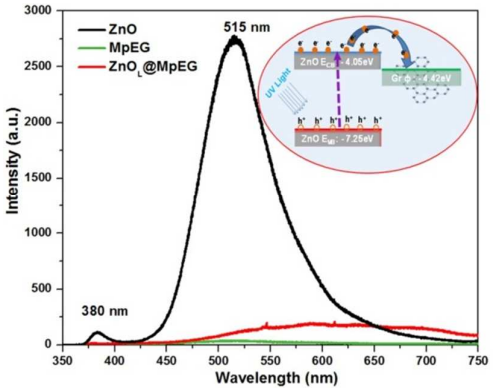

Figure 6: Photoluminescence spectra of ZnO, MpEG and ZnO$_L$@MpEG hybrids. Schematic image in inset represent the charge transfer and separation in the ZnO$_L$@MpEG hybrids.

The decrease in fluorescence yield of the band edge emission may be due to the interfacial charge transfer between ZnO and MpEG sheets[23, 43]. Thus there is no PL signature and the quenching phenomena occur. This may be ascribed to MpEG sheets in ZnO$_L$@MpEG hybrids material, become the separation center of the photo generated electrons and holes because these sheets are considered to be a good electron acceptor material to effectively hinder the electron–hole pairs recombination due to its 2D π-conjugation structure [46].

In order to illustrate the positive synergistic effect of the electrochemical performance, we analyse the electrochemical performance of the MpEG and ZnO$_L$@MpEG hybrids. For this, the cyclic voltammetry (CV) and charge discharge were performed in 1.0 M Na_2SO_4 electrolyte. Figure 7a shows that the CV curve of ZnO, MpEG and ZnO$_L$@MpEG hybrids curves at scan rate of 80 mV/s exhibit nearly rectangular shape. Also, indicating that ZnO$_L$@MpEG hybrids have largest integral area among the three samples, which indicates that the ZnO$_L$@MpEG hybrids material have positive synergistic effects in specific capacitance. The enhanced electrochemical performance of the ZnO$_L$@MpEG hybrids can be attributed to the thin deposited ZnO layer on MpEG sheets. Here, the MpEG in the hybrid electrode provides better electronic conductivity and excellent interfacial contact between ZnO layer and MpEG, which results in the fast transportation of electrons throughout the entire electrode matrix [47]. The specific capacitances [48] of electrodes were calculated using following equations:

$$Cs = \frac{\int IdV}{v \times m \times \Delta V} \qquad (1)$$

$$Cs = \frac{I \times \Delta t}{m \times \Delta V} \qquad (2)$$

where Cs is the specific capacitance of the electroactive materials (F/g), $\int IdV$ is the total integrated area of CV curve, I is the response current density (A/g), v is the scan rate (mV/s), m is the mass of the electroactive materials in the electrode (g), ΔV is the sweep potential window (V) and Δt is the discharge time (s).

The calculated values Cs using CV curves (using equation (1)) of ZnO, pristine MpEG, and ZnO$_L$@MpEG hybrids electrode are 280, 320 and 383 F/g, respectively, at a scan rate of 80 mV/s. The specific capacitance of the ZnO$_L$@MpEG hybrids electrode is found to be higher than that of the ZnO and MpEG. To further calculate the specific capacitance and study the rate capability of ZnO$_L$@MpEG hybrids electrode, the charge/discharge measurements (using equation (2)) were performed. Figure7b shows galvanostatic charge–discharge measurements of the ZnO$_L$@MpEG hybrids. This ZnO$_L$@MpEG hybrids electrode shows 472, 394, 358, 348 and 347 F/g at the current densities of 3.0, 3.5, 4.0, 4.5 and 5.0 A/g, respectively (Figure7c). With the increase of current densities, specific capacitance shows nearly constant behavior. These value is superior to those reported in previous studies for ZnO/RGO composite (303 F/g, at 10A/g) [49] and graphene/ZnO hybrid structures (316 F/g, at 6.7 A/g)[50], graphene/ZnO nanocomposites (109F/g, at 10 mV/s) [5], graphene-ZnO nanocomposite (146 F/g, at 2mV/s) [6], and graphene sheets anchored with ZnO nanocrystals (231 F/g, at 50 mV/s)[7]. It can be seen that the curves were nearly linear and exhibited a typical triangular shape even after a charging/discharging for more than 500 s, which indicated good electrochemical capacitive characteristics. The specific capacitance decreases with an increase in the current density from 3.0 to 5.0 A/g and this is may be due to the insufficient time available for ions to diffuse and adsorption inside smallest pores within a large particle at high current density.

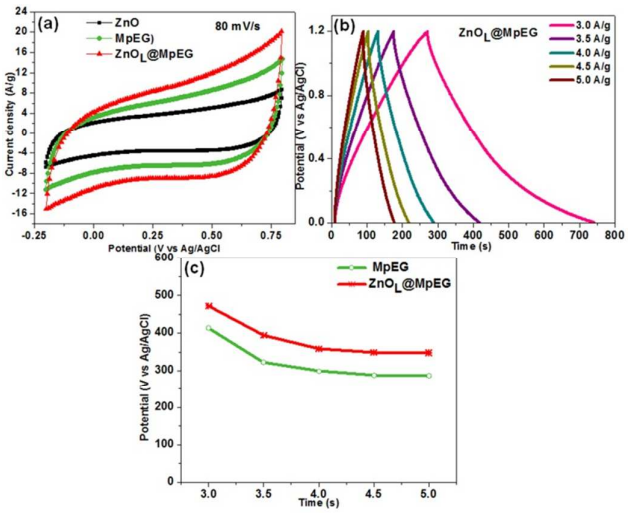

Figure 7: (a) Cyclic voltammetry of ZnO, MpEG and ZnO$_L$@MpEG hybrids at 80 mV/s, (b) charge-discharge of ZnO$_L$@MpEG hybrids and (c) specific capacitance of MpEG and ZnO$_L$@MpEG hybrids.

Figure 8 shows the schematic proposed mechanism for the formation of ZnO$_L$@MpEG hybrids in which ZnO nanoparticles forms the layer and deposited onto the surface of the MpEG. The functional groups attached on the basal plane are epoxy, hydroxyl and on the edges are carboxyl and carbonyl groups acts as the nucleation centers for the formation of ZnO onto MpEG sheets. When microwave is irradiated on the mixture of GO and zinc nitrate, it heats the reactant to a high temperature in a short time

by transferring energy selectively to microwave absorbing polar materials (Step-I). In-situ process, GO transforms into MpEG with porous nanostructures and simultaneously, zinc nitrate gets decomposed into Zn^{2+} ions. The functional groups attached on MpEG surfaces behave similar to negative charges and attract Zn ions towards it. The Zn^{2+} ions get attached on the MpEG surfaces since Zn^{2+} reacts with the functional groups on the MpEG, leading to the local creation of Zn–O–C and Zn-O bonding and binds on MpEG sheets (Step-II) [51]. The Zn^{2+} gets converted into ZnO nanoparticles by the help of oxygen content in the surrounding as well as functional groups on the MpEG sheets by absorbing thermal energy from microwave irradiation. Whole MpEG sheets are covered by ZnO nanoparticles in which functional group plays crucial role to bring them nearer to each other (Step-III). These ZnO nanoparticles cover the MpEG sheets from all sides uniformly because the incident microwave irradiation provides uniform heat on the surface of MpEG (Step-IV). In final stage these ZnO nanoparticles gets connected to each other on MpEG sheets and form the layered structure at high temperature which is delivered from microwave irradiation by transferring microwave energy. And thus the final structure of ZnO_L@MpEG hybrids is formed (Step-V).

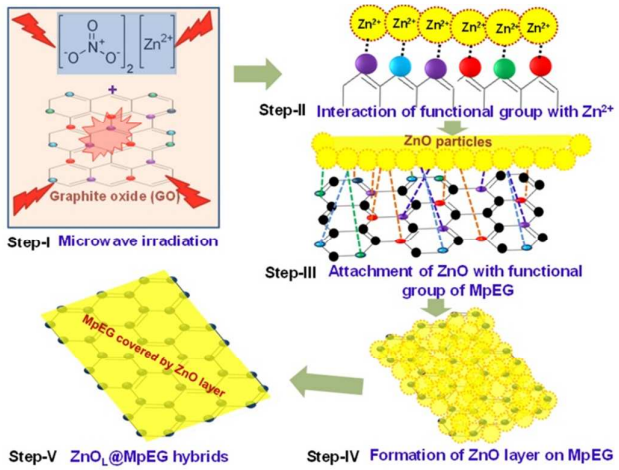

Figure 8: Mechanism of the formation of ZnO_L@MpEG hybrids. (i) Microwave irradiation on the mixture of GO and $(Zn(NO_3)_2$. Interaction between functional group and Zn^{2+} : Zn^{2+} interaction with negative functional group (iii) attachment of ZnO with functional group of MpEG (iv) formation of ZnO_L on MpEG and (v) ZnO_L@MpEG hybrids.

Conclusions

In summary, a basic technique to develop ultrathin ZnO layer onto microwave partially exfoliated graphene (MpEG) sheets prepared via a simple microwave irradiation method has been developed. After efficient microwave irradiation on the mixture of zinc nitrate and graphite oxide, it transform into ZnO_L@MpEG hybrids. The MpEG sheets have been successfully decorated by thin ZnO layers. The result shows that the MpEG sheets can facilitate the growth of ZnO layer on its surfaces in situ and improve the photoluminescence quenching and electrochemical properties. The obvious quenching phenomena observed from photoluminescence spectroscopy suggest that there is photo induced electron-transfer between ZnO layer and MpEG sheets. In comparison with the specific capacitance of MpEG electrode, the specific capacitance of ZnO_L@MpEG hybrid electrode is high. The combination of the ZnO layer with MpEG sheets enable hybrid to possess enhanced electrochemical behaviours and make them promising as electrode material for supercapacitor application.

Acknowledgements

SAM and ARV would like to acknowledge CNPq and FAPESP (Brazil) for financial support.

Notes and references

1. Z. Niu, L. Zhang, L. Liu, B. Zhu, H. Dong and X. Chen, *Adv. Mater.*, 2013, **25**, 4035.
2. Z. Li, B. Yang, K. Li, H. Wang, X. Lv, Y. Guo, Z. Zhang and Y. Su, *RSC Adv.*, 2014, **4**, 51640.
3. L. Dong, Z. Chen, D. Yang and H. Lu, *RSC Adv.*, 2013, **3**, 21183.
4. D. S. Dhawale, G. P. Mane, S. Joseph, S. N. Talapaneni, C. Anand, A. Mano, S. S. Aldeyab, K. S. Lakhi and A. Vinu, *RSC Adv.*, 2015, **5**, 13930.
5. A. Ramadoss and S. J. Kim, *Mater. Chem. Phys.*, 2013, **140**, 405.
6. T. Lu, L. Pan, H. Li, G. Zhu, T. Lv, X. Liu, Z. Sun, T. Chen and D. H. C. Chua, *J. Alloy. Compd.*, 2011, **509**, 5488.
7. C.-T. Hsieh, J.-S. Lin, Y.-F. Chen, C.-Y. Lin and W.-Y. Li, *Mate. Chem. Phys.*, 2014, **143**, 853.
8. D. Chu, Y. Masuda, T. Ohji and K. Kato, *Langmuir*, 2010, **26**, 2811.
9. T. Lv, L. Pan, X. Liu, T. Lu, G. Zhu and Z. Sun, *J. Alloy. Compd.*, 2011, **509**, 10086.
10. M. Willander, O. Nur, Q. X. Zhao, L. L. Yang, M. Lorenz, B. Q. Cao, J. Z. Pérez, C. Czekalla, G. Zimmermann, M. Grundmann, A. Bakin, A. Behrends, M. Al-Suleiman, A. El-Shaer, A. C. Mofor, B. Postels, A. Waag, N. Boukos, A. Travlos, H. S. Kwack, J. Guinard and D. L. S. Dang, *Nanotechnology*, 2009, **20**, 332001.
11. S. J. Pearton, D. P. Norton, Y. W. Heo, L. C. Tien, M. P. Ivill, Y. Li, B. S. Kang, F. Ren, J. Kelly and A. F. Hebard, *J. Electrom. Mater.*, 2006, **35**, 862.
12. B. Panigrahy and D.D. Shrma, *RSC Adv*., 2015, **5**, 8918.
13. M. Godlewski, E. Guziewicz, K. Kopalko, G. Łuka, M. I. Łukasiewicz, T. Krajewski, B. S. Witkowski and S. Gierałtowska, *Low Temp. Phys.*, 2011, **37**, 235.
14. A. Janotti and C. G. Van de Walle, *Phys. Rev. B*, 2007, **76**, 165202.
15. Ü. Özgür, Y. I. Alivov, C. Liu, A. Teke, M. A. Reshchikov, S. Doğan, V. Avrutin, S.-J. Cho and H. Morkoç, *J. Appl. Phys.*, 2005, **98**, 041301.
16. J. Yan, Q. Wang, T. Wei and Z. Fan, *Advanced Energy Materials*, 2014, **4**, 1300816.
17. K. S. Novoselov, V. I. Falko, L. Colombo, P. R. Gellert, M. G. Schwab and K. Kim, *Nature*, 2012, **490**, 192.
18. J. He, C. Niu, C. Yang, J. Wang and X. Su, *RSC Adv.*, 2014, **4**, 60253.
19. A. Wei, L. Xiong, L. Sun, Y. Liu, W. Li, W. Lai, X. Liu, L. Wang, W. Huang and X. Dong, *Mater. Res. Bull.*, 2013, **48**, 2855.

20. Y. J. Kim, H. Yoo, C. H. Lee, J. B. Park, H. Baek, M. Kim and G. C. Yi, *Adv. Mat.*, 2012, **24**, 5565.
21. T. Lv, L. Pan, X. Liu and Z. Sun, *Catal. Sci. Technol.*, 2012, **2**, 2297.
22. J. B. Park, W. Xiong, Z. Q. Xie, Y. Gao, M. Qian, M. Mitchell, M. Mahjouri-Samani, Y. S. Zhou, L. Jiang and Y. F. Lu, *Appl. Phys. Lett.*, 2011, **99**, 053103.
23. D. I. Son, B. W. Kwon, D. H. Park, W.-S. Seo, Y. Yi, B. Angadi, C.-L. Lee and W. K. Choi, *Nat. Nanotechnol.*, 2012, **7**, 465.
24. B. Li, J. Xu, J. Liu, S. Zuo, Z. Pan and Z. Wu, *J. Colloid Interf. Sci.*, 2012, **366**, 114.
25. T. Kavitha, A. I. Gopalan, K.-P. Lee and S.-Y. Park, *Carbon*, 2012, **50**, 2994.
26. R. Dwivedi, A. Maurya, A. Verma, R. Prasad and K. S. Bartwal, *J. Alloy. Compd.*, 2011, **509**, 6848.
27. G. Zhu, L. Pan, T. Xu and Z. Sun, *ACS App. Mater. Interf.*, 2011, **3**, 1472.
28. G. V. Bazuev, A. P. Tyutyunnik, I. F. Berger, I. V. Nikolaenko and B. G. Golovkin, *J. Alloy. Compd.*, 2011, **509**, 6158.
29. C. Hou, Q. Zhang, H. Wang and Y. Li, *J. Mater. Chem.*, 2011, **21**, 10512.
30. S. Park, J. An, J. R. Potts, A. Velamakanni, S. Murali and R. S. Ruoff, *Carbon*, 2011, **49**, 3019.
31. O. Lupan, G. A. Emelchenko, V. V. Ursaki, G. Chai, A. N. Redkin, A. N. Gruzintsev, I. M. Tiginyanu, L. Chow, L. K. Ono, B. Roldan Cuenya, H. Heinrich and E. E. Yakimov, *Mater. Res. Bull.*, 2010, **45**, 1026.
32. B. H. Bairamov, A. Heinrich, G. Irmer, V. V. Toporov and E. Ziegler, P*hys. Status Solidi B*, 1983, **119**, 227.
33. O. Akhavan, *ACS Nano*, 2010, **4**, 4174.
34. C. D. Wagner and G. E. Muilenberg, *Handbook of x-ray photoelectron spectroscopy: a reference book of standard data for use in x-ray photoelectron spectroscopy*, Physical Electronics Division, Perkin-Elmer Corp., 1979.
35. S. Y. Huang, Q. J. Cheng, S. Xu, D. Y. Wei, H. P. Zhou, J. D. Long, I. Levchenko and K. Ostrikov, *J. Appl. Phys.*, 2012, **111**, 036101.
36. J. Liqiang, W. Dejun, W. Baiqi, L. Shudan, X. Baifu, F. Honggang and S. Jiazhong, *J. Mol. Catal. A: Chem.*, 2006, **244**, 193-200.
37. J. Das, S. K. Pradhan, D. R. Sahu, D. K. Mishra, S. N. Sarangi, B. B. Nayak, S. Verma and B. K. Roul, *Physica B: Cond. Matter*, 2010, **405**, 2492.
38. H. Zhou and Z. Li, *Mater. Chem. Phys.*, 2005, **89**, 326.
39. J. Wu, X. Shen, L. Jiang, K. Wang and K. Chen, *Appl. Surf. Sci.*, 2010, **256**, 2826.
40. Y. Yang and T. Liu, *Appl. Surf. Sci.*, 2011, **257**, 8950.
41. A. van Dijken, E. A. Meulenkamp, D. Vanmaekelbergh and A. Meijerink, *J. Lumin.*, 2000, **90**, 123.
42. V. Subramanian, E. E. Wolf and P. V. Kamat, *J. Phys. Chem. B*, 2003, **107**, 7479.
43. G. Williams and P. V. Kamat, *Langmuir*, 2009, **25**, 13869.
44. N. Herring, S. Almahoudi, C. Olson and M. S. El-Shall, *J. Nanopart. Res.*, 2012, **14**, 1.
45. P. Roy, A. P. Periasamy, C.-T. Liang and H.-T. Chang, *Environ. Sci. Technol.*, 2013, **47**, 6688.
46. A. K. Geim, *Science*, 2009, **324**, 1530.
47. Y.-J. Kim, J.-H. Lee and G.-C. Yi, *Appl. Phys. Lett.*, 2009, **95**, 213101.
48. A. H. Nevidomskyy, G. Csányi and M. C. Payne, *Phys. Rev. Lett.*, 2003, **91**, 105502.
49. Y. Haldorai, W. Voit and J.-J. Shim, *Electrochim. Acta*, 2014, **120**, 65.
50. X. Dong, Y. Cao, J. Wang, M. B. Chan-Park, L. Wang, W. Huang and P. Chen, *RSC Adv.*, 2012, **2**, 4364.
51. S. Niyogi, E. Bekyarova, M. E. Itkis, J. L. McWilliams, M. A. Hamon and R. C. Haddon, *J. Am. Chem. Soc.*, 2006, **128**, 7720.